Mechanical properties and acoustic emission characteristics of coal samples with different fissure angle

Xuebin Gu
Shandong University of Science and Technology
Tongbin Zhao
Shandong University of Science and Technology
Weiyao Guo (363216782@qq.com)
Shandong University of Science and Technology
Xufei Gong
Shandong University of Science and Technology
Yongqiang Zhao
state key laboratory of water resource protection and utilization in coal mining
Yang Chen
shandong energy group co. ltd
Ninghui Xu
the geology and mineral resources of inner Mongolia co.ltd

Research

Keywords: Coal, Fissure angle, Mechanical properties, Acoustic emission, Spectrum analysis, Failure mode

Posted Date: September 7th, 2021

DOI: https://doi.org/10.21203/rs.3.rs-870741/v1

Abstract

To study the influence of fissure angle on the failure mechanism of coal mass, uniaxial compression tests were conducted on coal specimens with different fissure angles. The failure process and acoustic emission characteristics during loading were obtained. The mechanical properties and failure mode were further analyzed. The results showed that

(1) The stress-strain behavior of specimens with different fissure angles can be divided into four typical stages, compaction, elastic deformation, crack growth and propagation, and strain-softening. The existence of pre-existing fissures reduces the duration of the elastic stage with an obvious influence on the crack growth and propagation stage, and strain-softening stage.

(2) The uniaxial compressive strength, elastic modulus of the specimens containing pre-existing fissure are all lower than those of the unfissured. The strength and elastic modulus do not change significantly with fissure angle, which is closely related to the primary fracture of the coal.

(3) With the increase of the fissure angle, the crack initiation location moves from the center of the pre-existing fissure to the tip. While fissure angle has no obvious effect on the crack propagation direction, the cracks develop along the loading direction.

(4) The AE characteristics can be divided into three typical periods, quiet period, active period, and remission period. With the increase of the fissure angle, the duration proportion of the quiet period increases, indicating that the energy storage time of coal increases. With the increase of the fissure angle, the occurrence time of low frequency and high energy signal is delayed, indicating that the large-size rupture gradually concentrates in the late loading period.

(5) Compared with rock samples containing pre-existing fissure, coal specimens have more primary fractures, and the failure mechanism of coal is dominated by the non-uniform primary fractures.

1 Introduction

Due to geological tectonics and mining activities, there are a large number of joint, fissure, and structural plane defects in coal-rock mass (Li et al. 2021). The propagation and coalescence of cracks often lead to the failure of engineering coal and rock mass, which may cause dynamic instability (Tan et al. 2019; Tan et al. 2020). Therefore, the research on crack propagation, strength, and failure characteristics of jointed coal-rock material is of great significance to reveal the failure mechanism of the fractured rock mass.

A number of experimental and numerical investigations have been conducted for fractured rock. In terms of laboratory experiments, many studies have been carried out on the influence of the geometric distribution of pre-existing flaws on their mechanical properties. Yang et al. (2009, 2010) carried out uniaxial compression tests on fractured sandstone and marble, and investigated the effect of the layout of pre-existing flaws on the deformation and failure characteristics of the samples. Zhou et al. (2014) and Liu et al. (2015) studied the crack coalescence behavior in rock-like materials containing multiple flaws under uniaxial compression. Xiong et al. (2017) conducted uniaxial compression tests on sandstone samples containing two prefabricated fractures which interact with each other at the tip. Wang et al. (2018) carried out conventional uniaxial compression tests on low-strength fractured specimens with varying fracture numbers and apertures, and analyzed the stress-strain curve, strength, deformation parameters, and failure mode of each type of specimen in detail. Dou et al. (2020) conducted uniaxial compression tests on sandstone samples with precracks of different dip angles collected from a coal mine roof, and investigated how the crack dip angle affects the fracture mechanism. In terms of the influence of loading mode on its mechanics and failure characteristics, uniaxial loading tests are most commonly utilized(Yin et al. 2015; Hou et al. 2017; Luo et al. 2018; Guo et al. 2019; Yang et al. 2019). Besides, Wang et al. (2020) and Yang et al. (2021) carried out Brazilian splitting tests on pre-cracked disk specimens. Yu et al. (2020) studied the mechanical characteristics of sandstone samples with different loading rates and analyzed the effect of loading rate on the failure mechanism. Xiao et al. (2012, 2015) tested the crack growth and strength characteristics of samples with precracks under triaxial loading, and analyzed their failure mechanism based on the principle of fracture mechanics (Liu et al. 2016).

Numerous numerical simulations have also been carried out since it is repeatable and can provide more information about the internal cracks and mechanics (Zhang et al. 2013; Jiang et al. 2014; Tian et al. 2017). Huang and Yang (2014) used PFC^{2D} to simulate the red sandstone containing two pre-existing fissures under different confining pressures. Huang et al. (2019) combined laboratory tests and PFC software to study the fracture mechanism of a preexisting crack with a large opening, and pointed out that the failure of these large-opening crack specimens is mainly caused by the development of the shear secondary cracks instead of the tensile wing cracks.

Based on the above analysis, it can be concluded that the experimental objects are mainly rock materials such as sandstone and marble or rock-like materials, while the mechanical properties of coal samples containing pre-existing fissure are rarely studied. As a matter fact, the coal body typically contains more primary joints and is thereby more prone to instability failure under the action of load. The experimental study on the mechanical properties of coal containing fissure is of great importance to reveal the crack propagation and failure mechanism of coal. Therefore, we prefabricated fissures with different dip angles in real coal samples, and then carried out uniaxial compression tests, during which acoustic emission (AE) and video monitoring data were collected simultaneously. Based on the experiment results, the basic mechanical properties of the coal samples were analyzed. This paper is expected to provide a reference for the safe construction of underground engineering containing fractured coal.

2 Specimen Preparation And Testing Process

2.1 Specimen preparation

All samples were taken from a working face in Mine A located in western China. The coal is hard and matte black in texture. In order to maintain the original state, the samples were obtained from underground according to associated requirements and delivered to the laboratory for further processing. The coal was made into smooth-ended cylinders with a diameter of 50mm and a height of 100mm.Referring to the fissure manufacturing method in the literature (Liu et al. 2016), small-diameter round holes were firstly prefabricated with the mechanical machining method, and then the line cutting machine was used to cut through the small hole along the fissure direction, as shown in Fig. 1.

Three geometrical characteristics determine the geometry of a single fissure: fissure length 2l, fissure width d, and fissure angle α. Five fissure angles (α = 0°, 15°, 30°, 45°, and 60°), one fissure length(2l = 20mm) and one fissure width (d = 1mm) were involved in the tests. The samples are named with its fissure angle, 0°-1 represents the first sample with the fissure angle of 0°.

2.2 Testing system and process

As illustrated in Fig. 2, the experiment system includes a uniaxial testing system, an Acoustic emission system, and a video monitoring system. During a test, the three systems were started at the same time to expedite the post-processing of the test results.

The uniaxial tests were carried out using an RLJW-2000 rock testing equipment with an AMSY-6 acoustic emission system. The maximum compressional load capacity of the RLJW-2000 system is 2000 KN. In this test, the axial stress was controlled by the imposed axial displacement with a rate of 0.25 mm/min. The sampling frequency of the AE system is 10 MHz, and the threshold of recording is 40 dB. Two AE sensors were located at each side of the sample along the radial direction, and vaseline was used to enhance the coupling. Meanwhile, the video monitoring system, an EOS C100 camera, was used to capture images when the fractures appeared or failure occurred.

3 Basic Mechanical Characteristics And Failure Mode

3.1 Stress-strain curve

The stress-strain curve of the unfissured specimens (intact specimens) and those with pre-existing fissure are shown in Fig. 3. The stress-strain behavior of samples can be approximately divided into four typical stages, i.e. compaction, elastic

deformation, crack growth and propagation, and strain-softening.

Figure 3a shows the stress-strain curve features of the unfissured specimens. The specimen compressive strength is 32.8MPa. The stress-strain curve shows brittle characteristics when it reaches peak stress.At the stage of compaction, the curve shows the downward concave shape and the nonlinear deformation at the beginning of loading, which is related to the closure of some primary pores. At the stage of elastic deformation, the curve exhibits the characteristics of linear increases. At the stage of crack growth and propagation, the curve deviates from elastic behavior and exhibits clearly nonlinear deformation. At the stage of strain-softening, the stress-strain curves drop rapidly which is associated with the penetration of the macroscopic cracks.

Figure 3b shows the stress-strain curve features of the specimens with a fissure angle of 0°. The compressive strength is 9.55MPa (29.1% of the unfissured specimens). The stage of compaction and elastic are similar to that of the unfissured specimens. At the stage of crack growth and propagation and strain-softening, however, the stress fluctuates many times and the curves look like an irregular zigzag.

Figure 3c shows the stress-strain curve features of the specimens with a fissure angle of 15°. The specimen compressive strength is 6.47MPa (19.7% of the unfissured specimens). The strain of peak stress is about 0.75%, which is lower than that of the others. Compared with the unfissured specimens, the yield phenomenon of the specimens with a fissure angle of 15° is more obvious and the post-peak stress shows a step-like drop.

Figure 3d shows the stress-strain curve features of the specimens with a fissure angle of 30°. The specimen compressive strength is 12.6MPa (38.4% of the unfissured specimens). The stress-strain curve is similar to that of 15°. The yield phenomenon is obvious before the peak stress and the stress decreases in a step-like way after the peak value.

Figure 3e shows the stress-strain curve features of the specimens with a fissure angle of 45°. The specimen compressive strength is 8.14MPa (24.8% of the unfissured specimens). This angle shows different characteristics in the stage of strain-softening. Different from other angles, the coal samples with a fissure angle of 45° show the characteristics of multi-stage stress drop, and the proportion of post-peak curve increases significantly.

Figure 3f shows the stress-strain curve features of the coal specimens with a fissure angle of 60°. The specimen compressive strength is 16.4MPa (50% of the unfissured specimens). Except for the high stress at each stage, the stress-strain curve of the specimen is similar to that of 15° and 30°. The yield phenomenon appears before the peak value, and the post-peak stress decreases in a step-like manner.

Based on the above analysis, the stress-strain curve of the unfissured specimens and those with pre-existing fissure can be divided into four-stage: compaction, elastic deformation, crack growth and propagation, and strain-softening. Due to the existence of pre-existing fissures, the stage duration of elastic deformation is greatly reduced and the crack growth and propagation stage enters in advance. The stage of crack growth and propagation and strain softening show different characteristics as the change of the fissure angle. According to the difference of stress-strain curve, the specimens are divided into four types (A, B, C, D).

Type A: the stage of crack growth and propagation is approximately linear, and the post-peak behavior in stress-strain curves shows a rapid drop. The compressive strength of this type is high and a large amount of elastic energy is accumulated in the loading process, which indicates that this type of coal specimen has a strong dynamic failure tendency. The unfissured specimens belong to this type.

Type B: At the stage of crack growth and propagation, the curve presents obvious yield characteristics even accompanied by a small stress drop. At the stage of strain-softening, the curve decreases step by step. The specimens with fissure angles of 15°, 30°, and 60° belong to this type.

Type C: At the stage of crack growth and propagation and strain-softening, the stress-strain curves present an irregular zigzag pattern. The compressive strength of this type is low and less elastic energy is accumulated, which indicates that the dynamic failure trend of this type is very weak. The specimens with a fissure angle of 0° belong to this type.

Type D: The post-peak behavior in the stress-strain curves shows the characteristics of multi-stage stress drop and the duration of the post-peak part is relatively long. the specimens with a fissure angle of 45° belong to this type.

3.2 Strength and deformation characteristics

The uniaxial compressive stress (*UCS*), elastic modulus(*E*), and the strain of the peak stress (*Peak strain*) can effectively indicate the strength and deformation characteristics of the specimen. Therefore, we statistically analyzed these three parameters. Table 1 shows the basic mechanical parameters of specimens with different fissure angles. The relation among *UCS*, *E*, and *Peak strain* and fissure angle is shown in Fig. 4

Table 1
Mechanical parameters of specimens containing a single fissure under uniaxial compression

Specimen	UCS/MPa	Average value/MPa	Standard deviation	E/GPa	Average value/GPa	Standard deviation	Peak strain/%	Average value/%	Standard deviation
a-1	31.62	32.8	1.1800	1.76	1.74	0.0200	2.30	2.39	0.0882
a-2	33.98			1.72			2.47		
0°-1	10.16	9.55	0.4570	0.7	0.83	0.0990	2.46	1.77	0.5000
0°-2	9.43			0.85			1.56		
0°-3	9.06			0.94			1.30		
15°-1	6.38	6.47	0.0900	1.07	1.06	0.0050	0.79	0.79	0.0042
15°-2	6.56			1.06			0.78		
30°-1	12.14	12.60	0.4374	1.10	1.25	0.1040	1.68	1.53	0.1209
30°-2	13.19			1.31			1.52		
30°-3	12.48			1.33			1.38		
45°-1	9.03	8.14	0.6405	1.20	1.19	0.0094	0.98	0.87	0.0780
45°-2	7.56			1.18			0.84		
45°-3	7.82			1.20			0.79		
60°-1	18.61	16.4	1.6112	1.53	1.46	0.0741	1.82	1.65	0.1199
60°-2	15.79			1.5			1.55		
60°-3	14.81			1.36			1.58		

As shown in Fig. 4a, the *UCS* of different fissure angles do not show an obvious pattern, which may be closely related to the primary fractures in the coal. The unfissured specimens have a *UCS* of 32.8MPa, but specimens with a single fissure get a *UCS* of 6.47 MPa ($\alpha = 15°$) to 16.4MPa ($\alpha = 60°$), with a reduction between 50% and 80%. According to Fig. 4b, the existence of fissure also significantly weakens the elastic modulus, and the *E* of specimens with different fissure angles does not show an obvious pattern. The minimum value of the elastic modulus is 0.83GPa with the fissure angle of 0°. This is due to the fact that the normal to the fissure direction is parallel to the loading direction, and the deformation were much larger than the others during the loading process. The *Peak strain* of specimens with a single fissure are lower than that of unfissured specimens, as shown in Fig. 4c. The reason is that the presence of fissure destroys the integrity of the specimens, resulting in failure under low strain.

Base on the above analyses, *UCS*, *E*, and *Peak strain* of specimens containing pre-existing fissure are all lower than that of the unfissured samples. The variation of uniaxial compressive stress, elastic modulus under different fissure angles is not obvious, which is closely related to the primary fractures the coal.

3.3 Crack evolution process

To study the crack evolution process of coal specimens containing a pre-existing fissure, the video monitoring was adopted during the test. Based on the combined results on stress and video monitoring, the real-time crack evolution process of specimens was analyzed in detail.

Figure 5a shows the stress-strain curve of the specimens with a fissure angle of 0° and the corresponding crack propagation sketch. At the stages of compaction and elastic deformation, the pre-existing fissures did not produce a visually observable closure. When the stress reaches to point a(σ= 5.17MPa), the specimen initiates the crack from the center of the fissure, but the crack is small and inconspicuous. With the increase of stress, the crack widens a lot and the pre-existing fissure begins to close. At point c(σ= 7.34MPa), a new tensile crack forms quickly at the left tip of the fissure resulting a minor stress drop. Afterwards, the fissure has been closed. When the specimen is loaded to 7.49MPa (point d), two cracks begin to generate from the tip of the fissure and propagate along the axial stress. Finally, more cracks appear as the increase of deformation, resulting in the reduction of loading capacity.

Figure 5b shows the stress-strain curve of the specimens with a fissure angle of 15° and the corresponding crack propagation sketch. The stress reduction of the specimen mainly occurs in the post-peak stage, and the reduction usually corresponds to the macro crack propagation. When the stress reaches to point a(σ= 4.54MPa), the specimen initiates and propagate along the normal direction of the fissure. When the stress reaches 6.25MPa (point c), a crack generates near the under tip of the fissure. At point e(σ= 5.63MPa), the initial crack redevelops and propagates along the loading direction, corresponding to the significant decrease of stress. At this point, the pre-existing fissure has closed. Then, the stress gradually diminishes as the crack propagation on the left side of the specimen.

Figure 5c shows the stress-strain curve of the specimens with a fissure angle of 30° and the corresponding crack propagation sketch. It can be observed that stress drop in the stress-strain curve indicates a macro crack propagation. When the specimen is loaded to point a(σ= 9.61MPa), the specimen begins to initiate the wing crack 1,2 from the fissure, which can be seen with the naked eyes. When the stress is loaded to 12.22MPa (point e), the crack 3 emerges from the upper tip of the fissure and grows towards the loading direction, which presents an “H” type. At the point f, the pre-existing fissure has completely closed. When the specimen is loaded to point g(σ= 7.83MPa), cracks develop to the boundary, and the sample is expanded which leads to the loss of the bearing capacity.

Figure 5d shows the stress-strain curve of the specimens with a fissure angle of 45° and the corresponding crack propagation sketch. The pre-peak curve of the sample is smooth, and the post-peak stress presents a multistage decreasing trend. At point b(σ= 7.82MPa), the crack emanates from the lower tip of the fissure. When the stress reaches 6.71MPa (point d), a new crack develops quickly which leads to the expansion of the specimen. Then, the crack propagates downwards to the bottom when the stress reaches 5.96MPa (point f). Meanwhile, particles ejected from the right of the specimen, accompanied by an ejection sound. At this time, the fissure is almost close. With increasing axial deformation, the stress of the specimen steadily diminishes.

Figure 5e shows the stress-strain curve of the coal specimens with a fissure angle of 60° and the corresponding crack propagation sketch. As can be seen in the figure, macro cracks develop around the fissure from point a (σ= 13.95MPa) to point c(σ= 16.04MPa), during which many stress fluctuations occur. At point d (16.15MPa), coal ejection and fissure closure are observed. Afterward, when the coal is loaded to 18.61MPa (point g), coal ejection occurs once more, resulting in a rapid loss of supporting.

In brief, it can be concluded that the fissure angle has an effect on the initiation location of the initial crack. For the fissure angle of 0°, the initial crack is generated in the center of the pre-existing fissure. With the increase of fissure angle, the location

transfers to the tip of the fissure. According to the state of the pre-existing fissure, the failure process of the sample can be divided into two stages: the stage of fissure closure, and the stage of failure. In the stage of fissure closure, the cracks are generated around the fissure, mainly leading to the closure of the fissure. And the cracks generally propagate towards the loading direction. In the failure stage, the failure mode of the specimens is dominated by the comprehensive action of the primary fracture, pre-existing fissure, and the cracks initiated in the previous stage. And the coal specimens lose most of the bearing capacity due to structural failure.

3.4 Failure mode

To investigate the influence of the fissure angle on the failure mode of specimens, the failure pattern of coal specimens with fissure angles of 0°,15°,30°,45°,60° and without fissure were selected for analysis, as shown in Fig. 6.

Figure 6a shows the failure pattern of the coal sample with a fissure angle of 0°. It can be seen that the failure of this type is mainly caused by tensile cracks generated at the tips of the fissure, which is a typical tensile failure mode. Figure 6b gives the failure pattern with a fissure angle of 15°. The failure of the type is mainly the result of the upward development of the tensile wing cracks, and the failure mode is tensile. Figure 6c-e present the failure pattern with fissure angles of 30°, 45°, and 60°, respectively. There are obvious tensile and shear cracks in all of them, which indicates that the failure mode is a tensile-shear composite. At the same time, dynamic ejection also occurs during loading. The unfissured coal specimens is typically subject to splitting failure (Fig. 6f), indicating a tensile failure mechanism.

According to the above research, tensile failure occurs in the unfissured specimens and the specimens with a lower fissure angle. With the increase of the fissure angle, the failure mechanism alters to the composite failure of tensile and shear. Meanwhile, the dynamic ejection of particles gradually appears in the process of compression. For the fissure angles of 0° and 15°, there is no obvious ejection. For the fissure angles of 45° and 30°, large particle ejection occurs. For the fissure angle of 60°, there is an obvious dynamic ejection in the middle of the specimen.

4 Evolution Characteristics Of Acoustic Emission

4.1 AE counts and AE energy

Figure 7a-f present the relationship curves of time with stress, AE counts, and AE energy in uniaxial compression tests. AE counts is the number of waves that an AE signal exceeds the threshold, and AE energy reflects the area under the detection line of the signal (Li et al. 2017; Yuan et al. 2019). The AE characteristics of the unfissured and the specimens containing single fissure can be approximately divided into three typical periods, i.e. quiet period(□), active period(□) and remission period(□).

Figure 7a shows the AE characteristics of the specimens with fissure angle of 0°. The quiet period corresponds to the stage of compaction, and part of elastic deformation. Therefore, the AE counts and AE energy are relatively not very active. In the active period, and AE counts and AE energy of flawed specimens become active and have several larger peak values before peak stress. At the remission period, the AE counts and energy of specimen are very rare, and the stress decreases to a low level. It's worth noting that the absence of AE in the time range 400-600s is probably due to the propagation of the axial cracks. As shown in Fig. 7b-f, the AE evolution characteristics of specimens with fissure angle of 15° to unfissured specimens all present the following characteristics: few AE activities in the quiet period, massive in the active period, and rare in remission period.

The above research reveals that when the fissure angle grows, the duration proportion of quiet period increase. For the fissure angles of 0°, 15°, and 30°, the quiet period mainly corresponds to compaction stage of the stress-strain curve. For the fissure angles of 45° and 60°, the quiet period corresponds to the stage of compaction and partial elastic deformation, compaction and most elastic deformation, respectively. While the AE quiet period of the unfissured specimens covers the stage of compaction, elastic deformation, and partial crack growth and propagation. The duration proportion of quiet period increases, which indicates that the energy storage time of the specimen increases.

4.2 AE Spectral characteristics

The frequency spectral contain significant AE signal characteristics and are useful for learning more about cracks. AE energy also can be used to reveal the scale of rock rupture. By combined these two parameters simultaneously, it's possible to gain a better understanding of crack propagation (Zhang et al. 2016; Zhu et al. 2018). Based on the Fourier transform, all the dominant frequency of AE is calculated (Hu et al. 2018). While the AE energy was obtained by parameter analysis method. To analyze the relationships between frequency and AE energy, the date of domain frequency and the corresponding AE energy were exported in Fig. 8. An unfissured specimen, a specimen containing a 0° fissure and a specimen containing a 45° fissure were taken as examples to illustrate.

Figure 8 shows the correlation diagram of dominant-frequency and AE energy. The dominant frequency can be divided into three types: low frequency(20-130KHz), medium frequency (130-235KHz) and high frequency (235-330KHz). It can be observed that the normalized high-energy signal (≥0.12) is mostly located in the low frequency band, while the low-energy(≤0.12) is distributed in all the three bands. Accordingly, the signal can be divided into four types: low frequency and low energy (L-L), medium frequency and low energy (M-L), high frequency and low energy (H-L), low frequency and high energy (L-H). According to the assumption that high energy signal is related to large scale cracks, two rupture scale were classified, as shown in Table 2.

Table 2
AE energy and dominant-frequency characteristics of different rupture scales

Dominant-frequency characteristics	AE energy(normalized)	Signal characteristics	Rupture scale
low(20-130KHz)	low(≤0.12)	low frequency and low energy	small scale
low(20-130KHz)	high(≥0.12)	low frequency and high energy	large scale
medium(130-235KHz)	low(≤0.12)	medium frequency and low energy	small scale
high(235-330KHz)	low(≤0.12)	high frequency and low energy	small scale

Figure 9 presents the dominant frequency and stress changes during the test. The signal characteristics of the unfissured specimen is shown in Fig. 9(a). (A) At the stage of compaction and elastic deformation: in these two stages, there are three kinds of signals: L-L, M-L, H-L. Among them, the proportion of H-L signals is small. The center of the medium frequency band is approximately 160kHz, while the low frequency signals are clustered at 30kHz and 100kHz. And there is an empty band of low frequency between 30-100kHz. This indicates that due to the closure of original cracks and the development of microcracks, there are many failure modes in the specimen, but all of them are mainly small-scale ruptures. (B) At the stage of crack growth and propagation: medium frequency band signals increase, and the signal of empty band shows an increasing trend. At the same time, L-H signal appear with the frequency of 26kHz, 93kHz and 100kHz.The L-L signals dominate this stage, while the L-H signals also occur, indicating that the micro crack propagation forms large scale fractures. (C) At the stage of strain-softening: the occurrence of a large number of L-H signals indicates the rapid development of large-scale ruptures in the specimen, which corresponds to the rapid failure of the specimen. The specimens with a 0° fissure and a 45° fissure show a similar rule, but the difference is that the L-H signals appear earlier. The high energy signals of fissure angles of 0° and 45° appear around 90s and 160s, respectively, indicating that the occurrence time of large-scale cracks is earlier.

According to the above analysis, there are four types of signals in specimens. The L-H signals correspond to large-scale fractures. With the increase of fissure angle, the distribution of L-H signals gradually moves back. For example, the L-H signals of the unfissured coal samples approach the failure of the sample. It is shown that with the increase of fissure angle, the large-size rupture gradually concentrates in the late loading period.

5 Discussions And Insights

In Sect. 3.3, the crack evolution process of specimen containing single fissure is analyzed, and three types of initial crack are summarized (Type Ⅰ, Ⅱ, and Ⅲ), as shown in Fig. 10. Type Ⅰ: the crack which originates from the middle of the pre-existing fissure and develops toward the loading direction. This kind of crack is a tensile crack. Type Ⅱ: the initial crack starts at the tip

of the fissure, then develops in the direction of axial loading. This type also belongs to the tensile crack. It can be found in specimens with the fissure angles of 15°, 30°, 45° and 60°. Type Ⅱ: This type of crack is reverse to that of crack type Ⅰ, which is referred to as “anti-tensile crack”. The anti-tensile crack also initiates from upper or lower tips of fissure, and develops along the direction of the axial stress.

Yang and Jing (2010) studied the initial cracks of fractured sandstone with different fissure angels and found that there are more cracks of type Ⅰ, which was similar to the test results in this paper. Thus, the coal-rock material is characterized with a combination of high compressive and low tensile resistance. Yu et al. (2020) also carried out uniaxial compressive tests on sandstone with different fissure angles, and it was found that the initial crack also appeared in the center of the pre-existing fissure when the angle of 0°. It should be noted that type Ⅱ crack did not develop to the boundary of the specimens, indicating that it was not the main cause of specimen failure.

For coal specimens with pre-existing fissures, the strength and deformation parameters are lower than that of the unfissured specimens, and the strength of specimens with different fissure angles shows no obvious variation pattern. Yang et al. (2010) conducted uniaxial compressive tests on sandstone with various fissure angles and discovered that strength is the lowest when the fissure angle is 45°. This differs from the research in this paper. Compared with sandstone specimens, coal has more abundant primary fractures in its interior, which makes the mechanical parameters of different fissure angles not show a regular rule.

Pre-existing fissures can be regarded as obvious defects, which reduce the integrity of coal and lead to a significant decrease in its strength. There are abundant primary fractures in the coal, and the failure of specimens goes through the process of “crack initiation, crack propagation, crack coalescence, and macro-crack develop”. If the primary fracture is distributed along the growth path of the crack, the energy required to cause failure will be reduced, as shown in Fig. 11. The strength of the specimens fluctuates greatly due to the uneven distribution of the primary fracture, resulting in no obvious rule in the strength of specimens with varied fissure angles.

6 Conclusions

(1) The existence of the fissures can reduce the duration of elastic stage and has an influence on the stage of crack growth and propagation, and strain-softening. The uniaxial compressive strength, elastic modulus of coal samples containing pre-existing fissure are all lower than that of the unfissured samples. Compared with the unfissured specimens, the maximum strength reduction of fractured specimens is 80%, which is closely related to the primary fracture of the coal.

(2) The fissure angle of the specimens have a significant effect on the crack initiation location. When the fissure angle is 0°, the initiation crack occurs in the center of the pre-existing fissure. With the increase of the fissure angle, the crack initiation location transfers to the tip. While fissure angle has no obvious effect on the crack propagation direction, and the cracks develop along the loading direction.

(3) According to the evolution characteristics of acoustic emission, the loading process can be divided into quiet period, active period and remission period. With the increase of the fissure angle, the duration proportion of quiet period increases gradually, which means that the proportion of energy accumulation time increases, indicating that more energy can be stored in the specimen. With the increase of the fissure angle, the occurrence time of low frequency and high energy signal is delayed, indicating that the large-scale rupture gradually concentrates in the late loading period.

(4) Compared with the rock specimens containing a single pre-existing fissure, there are more primary fractures in the coal, and the non-uniform distribution of primary fractures plays a dominant role in controlling the failure mechanism of the coal specimens. This leads to the lack of obvious regularities in the strength of the coal specimens under the different fissure angle, indicating that the failure process of fractured coal specimens is different from that of the fractured rock.

Declarations

Acknowledgements

The research described in this paper was financially supported by the Major Program of Shandong Provincial Natural Science Foundation (No. ZR2019ZD13), Major Scientific and Technological Innovation Project of Shandong Provincial Key Research Development Program (No. 2019SDZY02) and National Natural Science Foundation of China (No. 51904165).

Compliance with ethical standards

Conflict of interest

The authors declare no conflicts of interest.

References

1. Dou L, Yang K, Chi XL (2020) Fracture behavior and acoustic emission characteristics of sandstone samples with inclined precracks. International Journal of Coal Science Technology 8(1):77–87
2. Guo QF, Wu X, Cai MF, Ren FH, Pan JL (2019) Crack initiation mechanism of pre-existing cracked granite. Journal of China Coal Society 44(S2):476–483
3. Hou ZK, Yang CH, Sun SW, Guo YT, Wang L, Xu F, Liu J (2017) Experiment and fracture mechanics analysis of plate shale under uniaxial compression. Journal of China Coal Society 42(5):1251–1257
4. Huang YH, Yang SQ (2014) Particle flow simulation of macro-and meso-mechanical behavior of red sandstone containing two pre-existing non-coplanar fissures. Chin J Rock Mechan Eng 33(8):1644–1653
5. Hung SB, Yao N, Ye YC, Cui XZ (2019) Strength and Failure Characteristics of Rocklike Material Containing a Large-Opening Crack under Uniaxial Compression: Experimental and Numerical Studies. International journal of geomechanics 19(8)
6. Hu XC, Su GS, Chen GY, Mei SM, Feng XT, Mei GX, Huang XH (2018) Experiment on Rockburst Process of Borehole and Its Acoustic Emission Characteristics. Rock Mech Rock Eng 52(3):783–802
7. Jiang MJ, Chen H, Zhang N, Fang R (2014) Distinct element numerical analysis of crack evolution in rocks containing pre-existing double flaw. Rock Soil Mechanics 35(11):3259–3268
8. Li HG, Li HM (2017) Mechanical properties and acoustic emission characteristics of thick hard roof sandstone in Shendong coal field. International Journal of Coal Science Technol 4(2):147–158
9. Li WZ, Kang HP, Jiang ZY, Si LP, Cai RC, Guo GY (2021) Deformation failure mechanism of fractured deep coal-rock mass and high-pressure grouting modification strengthening testing. Journal of China Coal Society 46(3):912–923
10. Liu QS, Xu J, Liu XW, Jiang JD, Liu B (2015) The role of flaws on crack growth in rock-like material assessed by AE technique. Int J Fract 193(2):99–115
11. Liu WT, Shen JJ (2016) Experimental study of propagation mode of crack in real rock specimens with a single crack. Chin J Rock Mechan Eng 35(6):1182–1189
12. Luo K, Zhao GD, Zeng JJ, Zhang XX, Pu CZ (2018) Fracture experiments and numerical simulation of cracked body in rock-like materials affected by loading rate. Chin J Rock Mechan Eng 37(8):1833–1842
13. Tan YL, Guo WY, Xin HQ, Zhao TB, Yu FH, Liu XS (2019) Key technology of rock burst monitoring and control in deep coal mining. Journal of China Coal Society 44(1):160–172
14. Tan YL, Guo WY, Zhao TB, Meng XJ (2020) Coal rib burst mechanism in deep roadway and “stress relief-support reinforcement” synergetic control and prevention. Journal of China Coal Society 45(1):66–81
15. Tian WL, Yang SQ, Huang YH (2017) PFC2D simulation on crack evolution behavior of brittle sandstone containing two coplanar fissures under different confining pressures. Journal of Mining Safety Engineering 34(6):1207–1215

16. Wang H, Li Y, Cao SG, Pan RK, Yang HY, Zhang KW, Liu YB (2020) Brazilian splitting test study on crack propagation process and macroscopic failure mode of pre-cracked black shale. Chin J Rock Mechan Eng 39(5):912–926
17. Wang YL, Tang JX, Dai ZY, Yi T, Li XY (2018) Effect of fracture number and aperture on mechanical properties and failure modes of low-strength rock mass. Journal of China Coal Society 43(12):3338–3347
18. Xiao TL, Li XP, Jia SP (2012) Triaxial test research and mechanical analysis based on structure surface effect of deep rock mass with single fissure. Chin J Rock Mechan Eng 31(8):1666–1673
19. Xiao TL, Li XP, Jia SP (2015) Triaxial test research of failure characteristic with two pre-existing transfixion cracks. Chin J Rock Mechan Eng 34(12):2455–2462
20. Xiong F, Jing HW, Su HJ, Du MR, Yin Q, Han GS (2017) Strength and fracture behaviors of sandstone samples containing intersect fissures under uniaxial compression. Journal of China Coal Society 42(4):886–895
21. Yang DF, Zhang DY, Niu SJ, Ge SS, Liu S, Chen X, Wang TT, Li XY (2019) Experimental study on crack propagation process and macroscopic failure mode of prefabricated-crack fine sandstone under uniaxial compression. Journal of Mining Safety Engineering 36(4):786–793
22. Yang SQ, Dai YH, Han LJ, He YN, Li YS (2009) Uniaxial compression experimental research on deformation and failure properties of brittle marble specimen with pre-existing fissures. Chin J Rock Mechan Eng 28(12):2391–2404
23. Yang SQ, Jing HW (2010) Strength failure and crack coalescence behavior of brittle sandstone samples containing a single fissure under uniaxial compression. Int J Fract 168(2):227–250
24. Yang SQ, Zhang PC, Teng SY, Tian WL, Huang YH (2021) Experimental study of tensile strength and crack evolution characteristics of Brazilian discs containing three pre-existing fissures. Journal of China University of Mining Technology 50(1):90–98
25. Yin PF, Yang SQ, Zeng W (2015) A Simulation Study on Strength and Crack Propagation Characteristics of Layered Composite Rock With Single Fissure. Journal of Basic Science Engineering 23(3):608–621
26. Yu LQ, Yao QL, Xu Q, Wang WN, Niu ZJ, Liu WD (2020) Experimental and numerical simulation study on crack propagation of fractured fine sandstone under the influence of loading rate. Journal of China Coal Society 1–15
27. Yuan RF, Shi BW (2018) Acoustic emission activity in directly tensile test on marble specimens and its tensile damage constitutive model. International Journal of Coal Science Technology 5(3):295–304
28. Zhang XP, Wong LNY (2013) Crack Initiation, Propagation and Coalescence in Rock-Like Material Containing Two Flaws: A Numerical Study Based on Bonded-Particle Model Approach. Rock Mech Rock Eng 46(5):1001–1021
29. Zhang YB, Liang P, Tian BZ, Yao XL, Sun L, Liu XX (2016) Multi parameter coupling analysis of acoustic emission signals of granite disaster and the precursor characteristics of the main rupture. Chin J Rock Mechan Eng 35(11):2248–2258
30. Zhou XP, Cheng H, Feng YF (2014) An Experimental Study of Crack Coalescence Behavior in Rock-Like Materials Containing Multiple Flaws Under Uniaxial Compression. Rock Mech Rock Eng 47(6):1961–1986
31. Zhu ZF, Chen GQ, Xiao HY, Liu H, Zhao C (2018) Study on crack propagation of rock bridge based on multi parameters analysis of acoustic emission. Chin J Rock Mechan Eng 37(4):909–918

Figures

Fig. 1 Geometry of single fissure in the coal samples

Figure 1

See image above for figure legend.

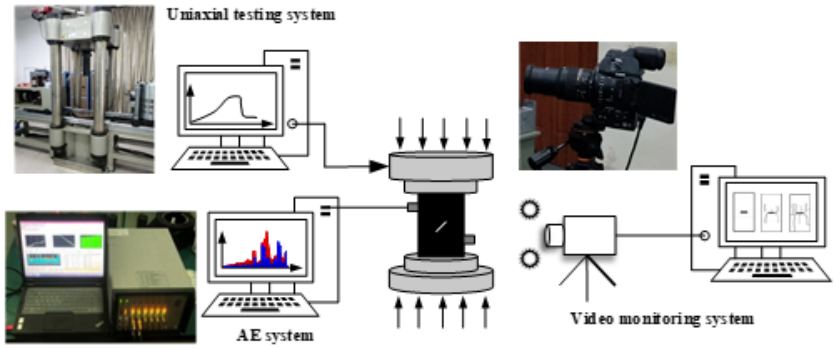

Fig. 2 The experiment system

Figure 2

See image above for figure legend.

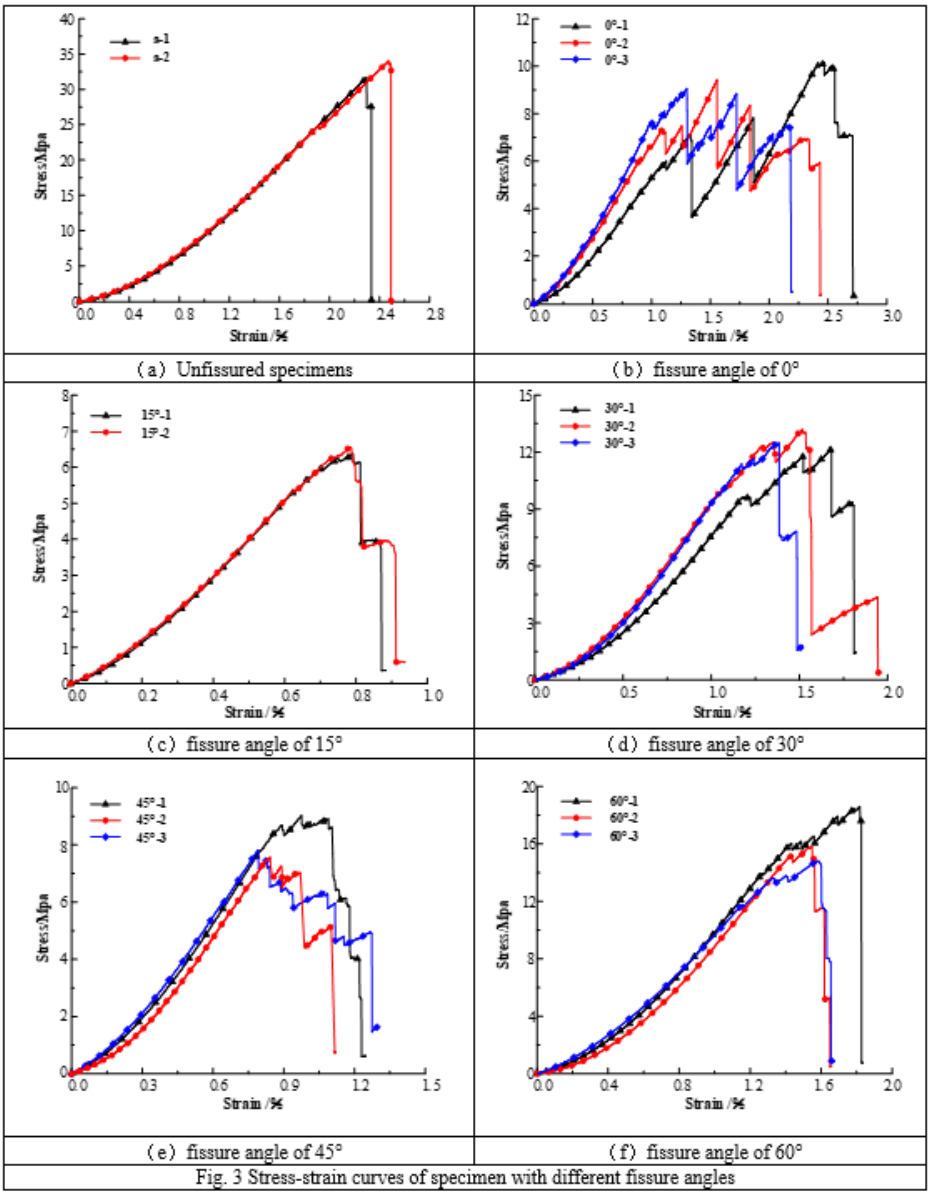

Fig. 3 Stress-strain curves of specimen with different fissure angles

Figure 3

See image above for figure legend.

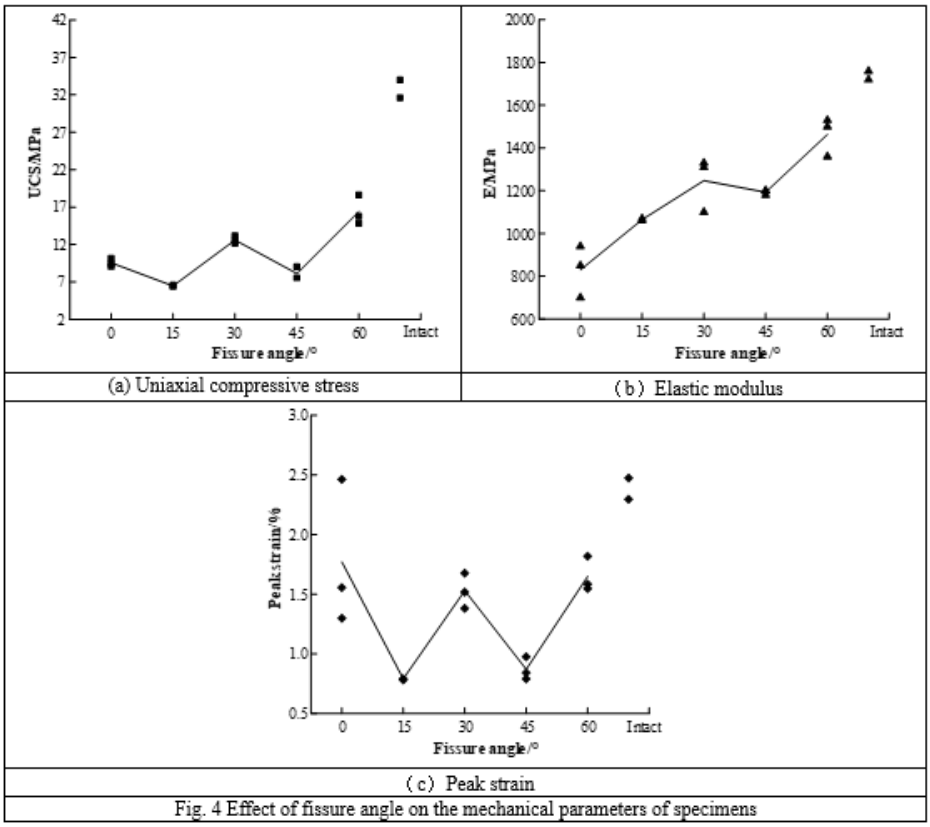

Fig. 4 Effect of fissure angle on the mechanical parameters of specimens

Figure 4

See image above for figure legend.

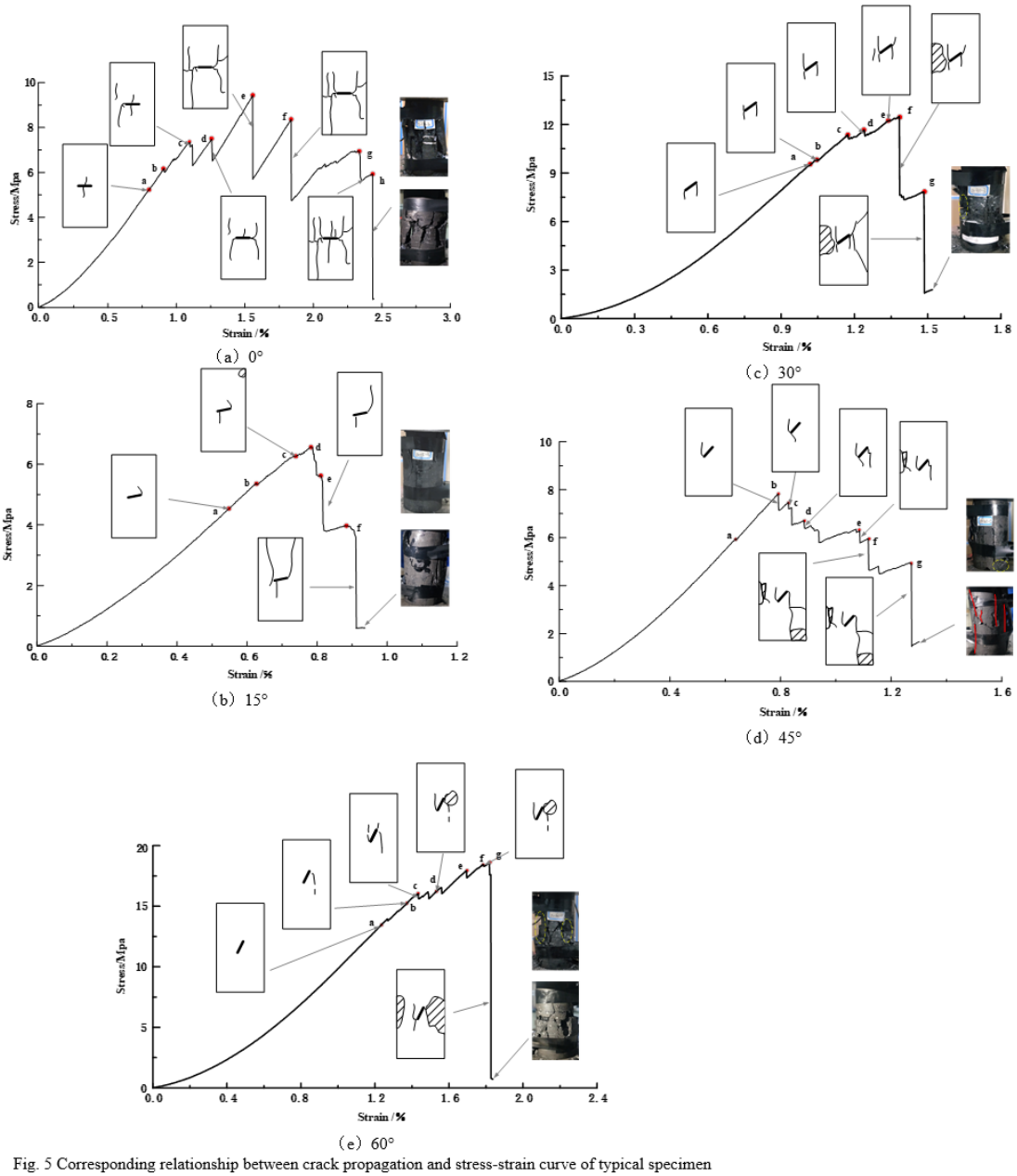

Fig. 5 Corresponding relationship between crack propagation and stress-strain curve of typical specimen

Figure 5

See image above for figure legend.

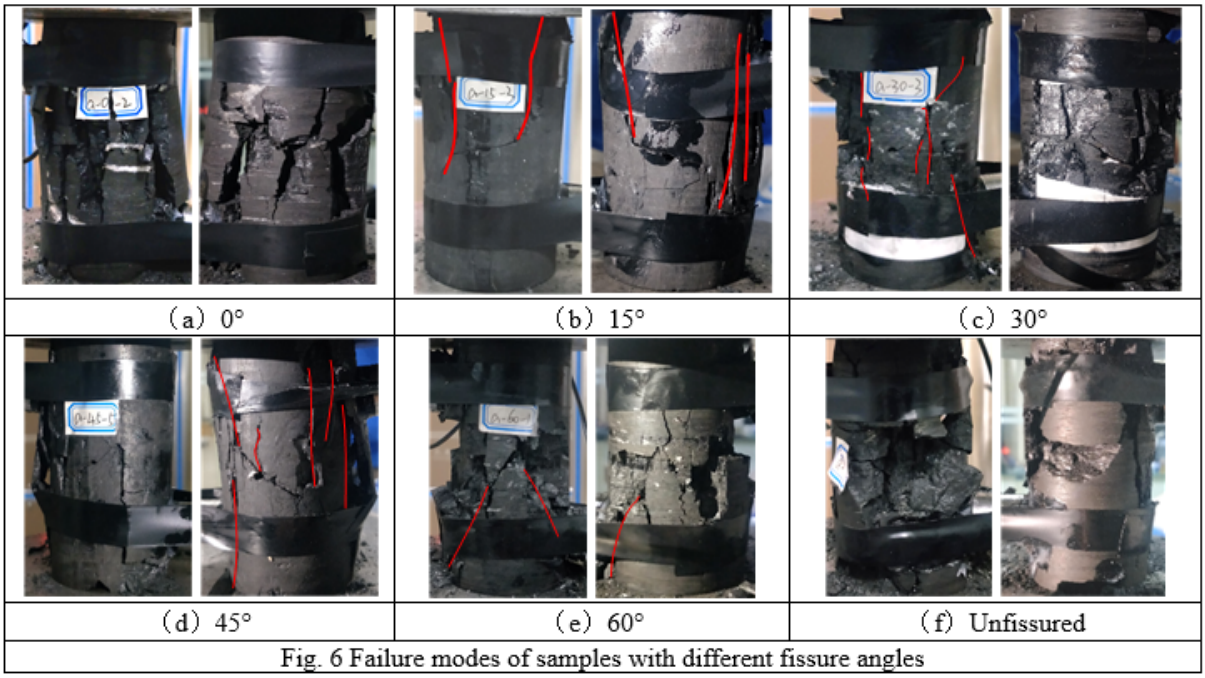

Fig. 6 Failure modes of samples with different fissure angles

Figure 6

See image above for figure legend.

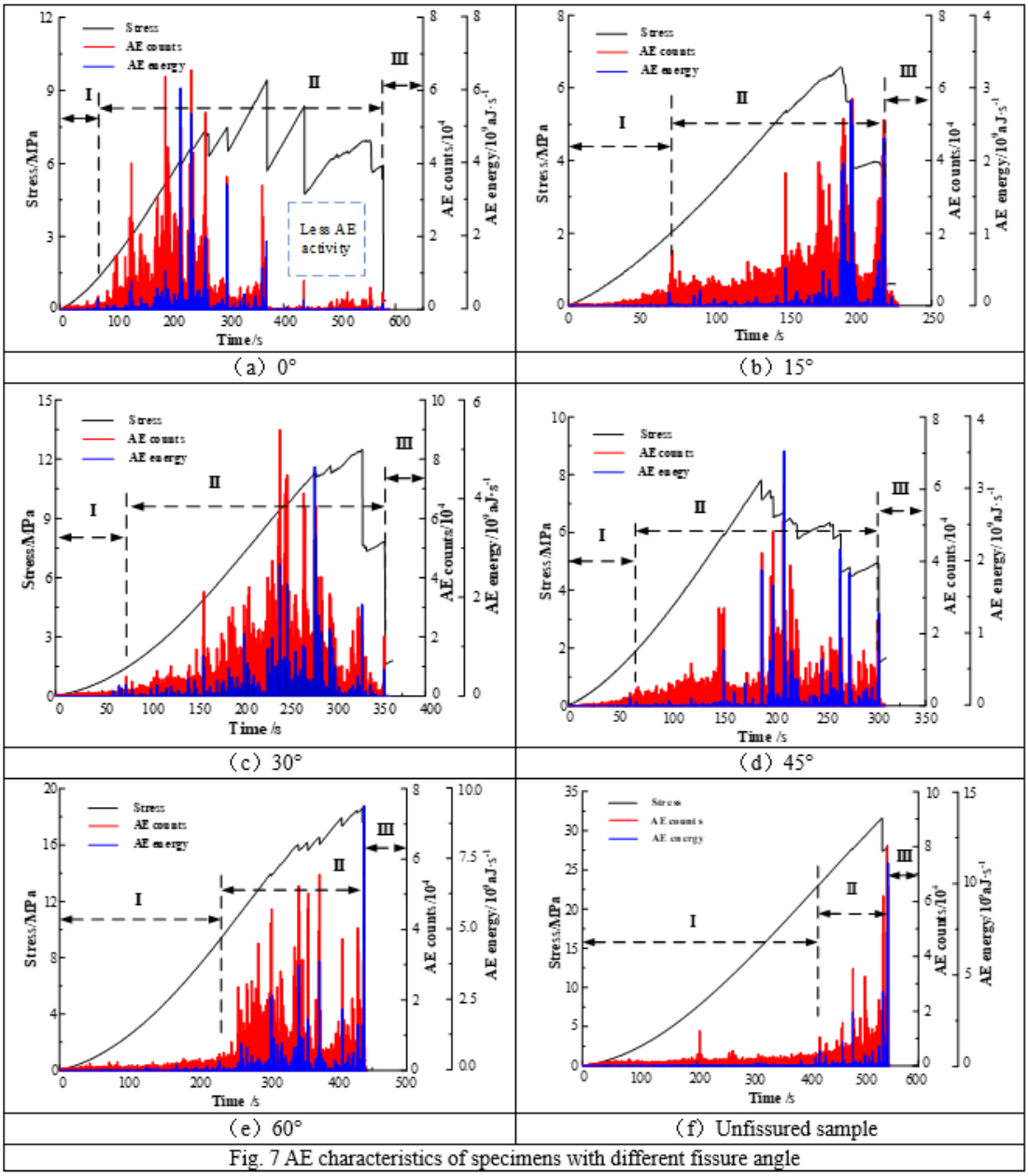

Fig. 7 AE characteristics of specimens with different fissure angle

Figure 7

See image above for figure legend.

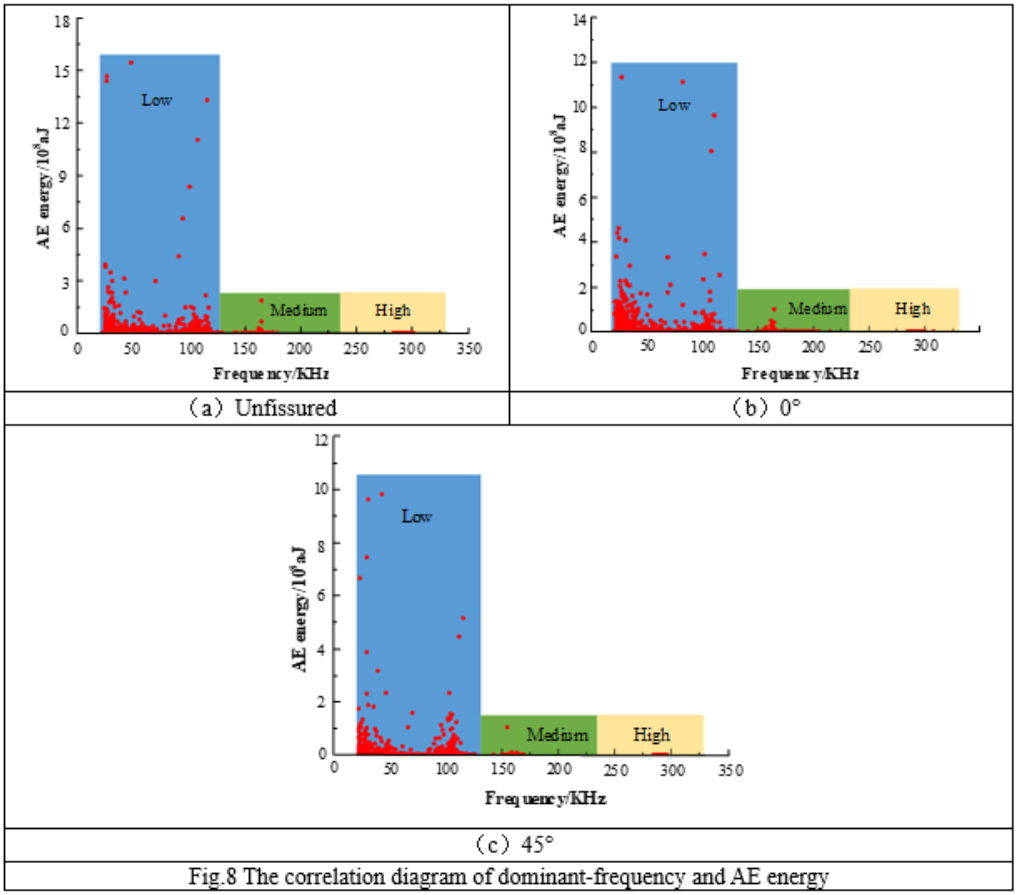

Fig.8 The correlation diagram of dominant-frequency and AE energy

Figure 8

See image above for figure legend.

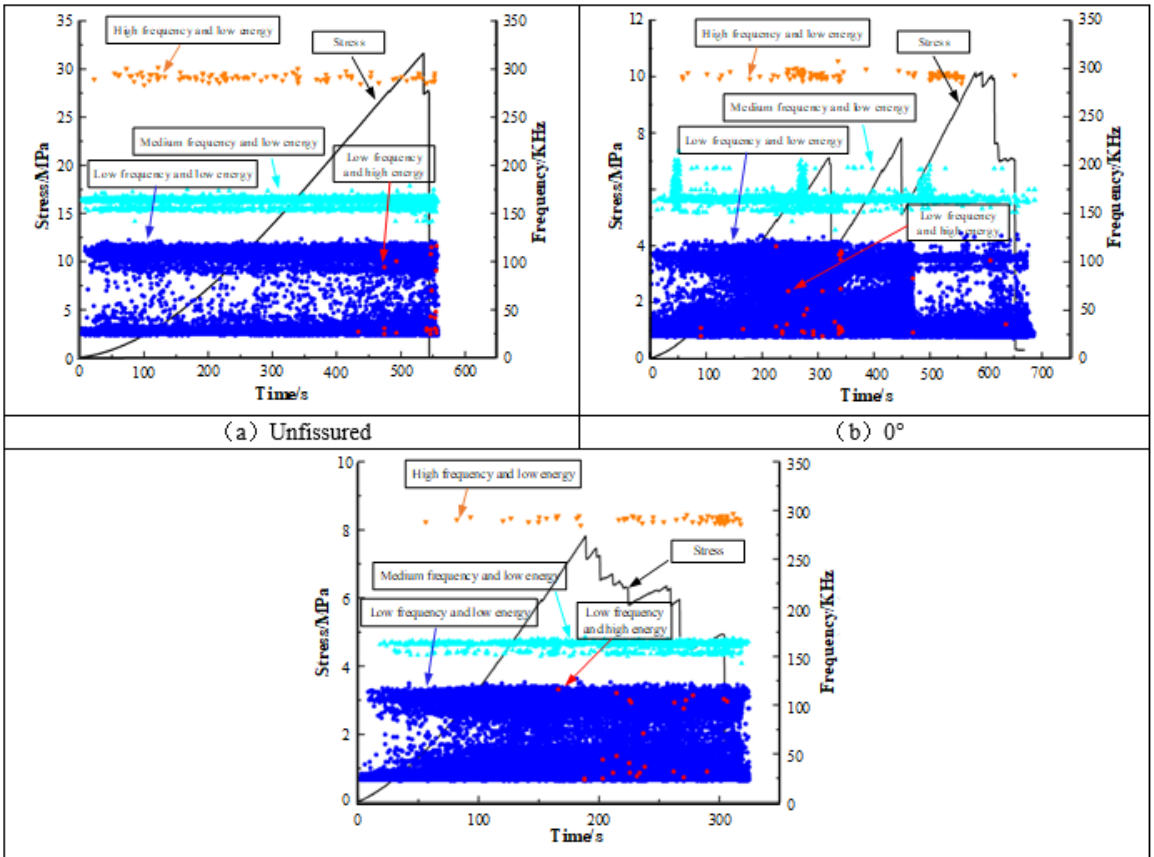

Fig.9 Dominant frequency and stress changes in the process of samples failure

Figure 9

See image above for figure legend.

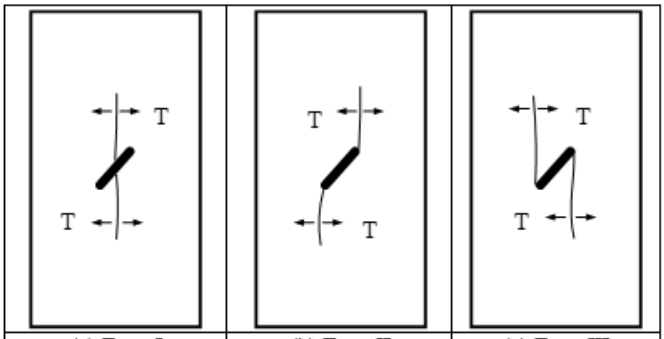

(a) Type I (b) Type II (c) Type III

Fig. 10 Types of initial crack

Figure 10

See image above for figure legend.

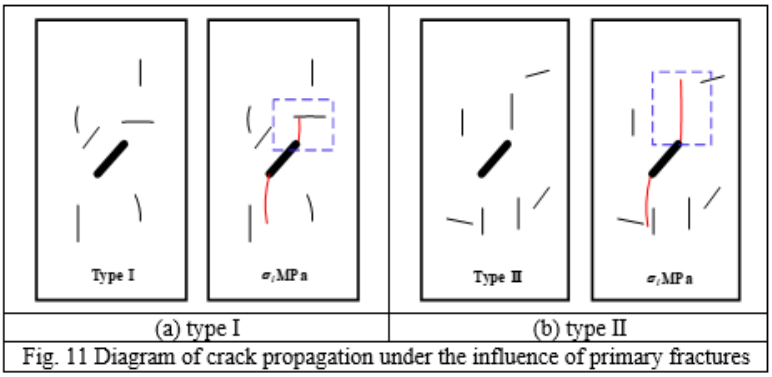

(a) type I (b) type II

Fig. 11 Diagram of crack propagation under the influence of primary fractures

Figure 11

See image above for figure legend.